J Supercond Nov Magn (2012) 25:45–53
DOI 10.1007/s10948-011-1207-4

ORIGINAL PAPER

Effect of MgO Nano-oxide Additions on the Superconductivity and Dielectric Properties of $Cu_{0.25}Tl_{0.75}Ba_2Ca_3Cu_4O_{12-\delta}$ Superconducting Phase

N.H. Mohammed

Received: 15 May 2011 / Accepted: 21 June 2011 / Published online: 23 August 2011

Abstract The effect of MgO nano-oxide on both superconducting and dielectric properties of polycrystalline $(Cu_{0.25}Tl_{0.75})$-1234 was studied. The MgO-content varied from $x = 0.0$ up to 1.0 wt% of the sample's total mass. The volume fraction of the prepared samples ($x = 0.0$, 0.2, 0.6 and 1.0 wt%) was estimated from the room-temperature X-ray powder diffraction patterns. The superconducting transition temperature T_c, calculated from resistivity data, increased from 122 to 136 K as x increased from 0.0 to 0.8 wt% and then it decreased to 117 K for $x = 1.0$ wt%. Also, the dielectric properties of all samples were measured in the frequency range from 100 Hz to 4 MHz at different temperatures from 113 to 300 K. The real part of dielectric constant ε' was strongly dependent on both temperature and frequency for all x values. The imaginary part of dielectric constant ε'' and loss factor $\tan\delta$ showed dispersion which shift toward lower frequencies with decreasing temperature. The ac conductivity σ_{ac} was derived from the admittance and sample dimensions in the same frequency range. It followed the power law $\sigma_{ac}(\omega) \sim \omega^{-\gamma}$ with $\gamma \approx 0.8$.

Keywords (Cu,Tl)-1234 · MgO nano-particles · Dielectric constants · Loss factor

1 Introduction

The crystal structure of $(Cu_{1-x}Tl_x)$-1234 superconducting phase is a tetragonal unit cell and it has four CuO_2-planes, acting as a conduction band, whereas the charge reservoir of $(Cu_{1-x}Tl_x)$-1234 is $Cu_{1-x}Tl_xBa_2O_{4-\delta}$ [1]. $(Cu_{1-x}Tl_x)$-1234 superconducting phase was prepared by Ihara et al. [2] under a high pressure of 3.5 GPa and low pressure of 0.1 GPa at 950–1100 °C for 1–3 hours in a gold capsule. They found that the superconducting transition temperature T_c for this phase was higher than that of Cu-1234 and Tl-1234 by 8 K and 4 K, respectively. Also, the anisotropy parameter for $(Cu_{1-x}Tl_x)$-1234 was found to be almost identical to that of Tl-1234 phase [3] and smaller than that of Cu-1234 [4]. Unfortunately, the high-pressure synthesis technique is not economical for practical applications. So, Khan et al. [1] reported a simple and direct method for $(Cu_{1-x}Tl_x)$-1234 synthesis at ambient pressure based on two steps of solid-state reaction technique. A single phase of $(Cu_{1-x}Tl_x)$-1234 was achieved at T_c around 120 K and zero resistivity temperature T_0 of about 106 K. The first chemical substitution in this phase was performed by Khan et al. [5], who substituted Be at Ca-site to improve the interplanar coupling. This study showed that Be-substitution at Ca-site contracted the lattice parameter c and the post-air annealing increased the oxygen content. Also, in a previous work, Mohammed et al. [6] had successfully synthesized $Cu_{0.25}Tl_{0.75}Ba_2Ca_{3-y}Er_yCu_4O_{12-\delta}$ superconducting phase by a single step of a solid-state reaction technique at ambient pressure and studied the effect of Er-substitution at Ca-site on its physical properties. It was found that the small content of Er ($0.0 \le y \le 0.05$) decreased the transition width and this result was attributed to the enhancement of volume fraction of this phase. Awad [7] studied the effect of MgO nano-oxide on the electrical and mechanical properties of $Cu_{0.25}Tl_{0.75}Ba_2Ca_3Cu_4O_{12-\delta}$ superconducting phase. He found that the lower concentration of MgO nano-addition to $(Cu_{0.25}Tl_{0.75})$-1234 phase improved the critical current density J_c, enhanced both T_c and the Vick-

N.H. Mohammed (✉)
Physics Department, Faculty of Science, Alexandria University, Alexandria, Egypt
e-mail: nhmohammed@yahoo.com

ers microhardness and enhanced the volume fraction of the formed phase.

The high dielectric constant of high-temperature superconductors found numerous technological applications. Recently, materials with giant dielectric constant played an increasingly significant role in the growth of microelectronics because of the desire for smaller and more robust devices such as capacitors and memory devices [8]. In the case of memory devices based on capacitive components, such as static and dynamic random access memories, the static dielectric constant will ultimately decide the level of miniaturization [9]. The higher values of the dielectric constant were observed in many high-temperature superconductors [8, 10–20]. So with the advent of these HTSC compounds, the field of electronics had a great deal of potential in using this technology for a variety of applications. Relatively higher values of dielectric constants were reported for $Bi_2Ba_2Nd_{1.6}Ce_{0.4}Cu_2O_{10+\delta}$ [8], $Tl_2Ba_2CaCu_2O_{8-\delta}$ [10], $Tl_2Ba_2Ca_2Cu_3O_{10-\delta}$ [10], $Bi_{1.84}Pb_{0.34}Sr_{1.9}Ca_{2.03}Cu_{3.06}In_xO_{10+\delta}$ [11] and $Cu_{0.5}Tl_{0.5}Ba_2Ca_{2-x}Cd_xCu_3O_{10-\delta}$ [20] superconductors. Furthermore, Mumtaz et al. [21, 22] studied the dielectric properties of $Cu_{0.5}Tl_{0.5}Ba_2(Ca_{2-y}Mg_y)(Cu_{0.5}Zn_{2.5})O_{10-\delta}$ and $Cu_{0.5}Tl_{0.5}Ba_2Ca_3Cu_4O_{12-\delta}$ bulk superconductors in the range of 10 KHz to 10 MHz and a negative capacitance (NC) phenomenon was observed. Also a similar phenomenon (NC) was observed by Cavdar in $Tl_2Ba_2CaCu_2O_{8-\delta}$ [10]. It is well known that there are four primary mechanisms of polarization in materials. Electronic polarization, atomic and ionic polarization, dipolar or oriental polarization and interfacial polarization, and each mechanism involves a short-range motion of charges and contribute to the total polarization of the material.

In this work, the effect of MgO nano-oxide additions on the superconductivity and dielectric properties of $Cu_{0.25}Tl_{0.75}Ba_2Ca_3Cu_4O_{12-\delta}$ superconducting phase was studied. The real and imaginary parts of dielectric constant ε' and ε'', dielectric loss factor $\tan\delta$ and ac conductivity σ_{ac} for $(MgO)_xCu_{0.25}Tl_{0.75}Ba_2Ca_3Cu_4O_{12-\delta}$ samples with $x =$ 0.0 wt%, 0.2 wt%, 0.4 wt%, 0.6 wt%, 0.8 wt% and 1.0 wt% were calculated using the capacitance C_p, conductance G and admittance Y measurements in the frequency range of 100 Hz to 4 MHz and at different temperatures from 113 K to 300 K.

2 Experimental Technique

Samples with the nominal composition of $Cu_{0.25}Tl_{0.75}Ba_2Ca_3Cu_4O_{12-\delta}$ with different added amounts of nano-oxide MgO (0.0–1.0 wt%) were prepared by a single step solid-state reaction technique at ambient pressure. Amounts of Tl_2O_3, BaO_2, CaO and CuO were used to prepare a sample of about 2.1 g with nominal compositions as 0.75:2:3:4.25. These compositions were ground in an agate mortar and then were sifted by a 65 μm sieve. After sieving, the nano-oxide MgO (40 nm, Sigma Aldrich) was added as a weight % to the sifted powder. The powder was pressed into a disc (diameter of 1.5 cm and thickness of about 0.3 cm), and then the disc was wrapped in a silver foil to minimize the thallium losses during the sintering process. The samples were heated in a sealed quartz tube (1.8 cm diameter and 12 cm long) at a rate of 2 °C/min to 780 °C, followed by a heating rate of 1 °C/min to 860 °C, and finally held at this temperature six hours. At the end of this period, the samples were slowly cooled to room temperature.

The samples were characterized by X-ray powder diffraction (XRD) using Shimadzu 7000 with Cu K_α-radiation ($\lambda =$ 1.5418 Å) in the range $20° \leq 2\theta \leq 60°$. The grain size and homogeneity of the samples were identified using a Jeol scanning electron microscope JSM-5300, operated at 30 kV, with a resolution power of 4 nm. Energy dispersive spectroscopy (EDS) analysis were performed for the prepared samples using an Oxford X-ray micro-probe analysis connected to Jeol scanning microscope JSM-5300.

The electric resistivity of the prepared samples was measured by the conventional four-probe technique from room temperature down to T_0 via a closed cryogenic system, employing helium gas as a working medium. The samples had the shape of parallelepipeds of approximate dimensions $1.5 \times 0.2 \times 0.3$ cm^3, and a conductive silver paint was used for the connections of copper leads with the sample. The temperature of the sample was monitored by a chromel versus Fe-Au thermocouple and stabilized with the aid of a temperature controller to within ±0.1 K. A typical excitation of 1 mA was used to avoid heating effects on the samples. The potential drop across the sample was measured using a Keithly 181 digital nano-voltmeter. The voltage was determined by taking the average of the values measured with the normal and reverse directions of applied current to eliminate the thermoelectric voltage of the junction leads.

The frequency dependent dielectric measurements were performed using Hioki-3532 LCR Hitester from $f = 100$ Hz to 4 MHz at different temperatures. Silver paint was painted in both sample surfaces and dried at room temperature. The sample is heated at 180 °C for one hour to ensure the good contact between silver metal and superconductor sample. Two copper leads were attached to the silver electrode surface to measure the capacitance. By measuring the capacitance C_p, conductance G and admittance Y for the prepared samples with different MgO nano-concentrations. The real and imaginary parts of dielectric constant ε' and ε'', dielectric loss factor $\tan\delta$ and ac conductivity σ_{ac} of the prepared samples were calculated using the following rela-

tions:

$$\varepsilon' = \frac{c_p d}{A\varepsilon_0} \tag{1}$$

$$\tan\delta = \frac{G}{c_p \omega} \tag{2}$$

$$= \frac{\varepsilon''}{\varepsilon'} \tag{3}$$

$$\sigma_{ac} = \frac{Yd}{A}, \tag{4}$$

where Y is the admittance ($Y = 1/Z$, Z is the impedance in Ω), d is the thickness of the sample (m), A is the area of the electrode (m^2), ε_0 is the permittivity of free space ($\varepsilon_0 = 8.85 \times 10^{-12}$ F/m) and ω ($=2\pi f$) is the angular frequency.

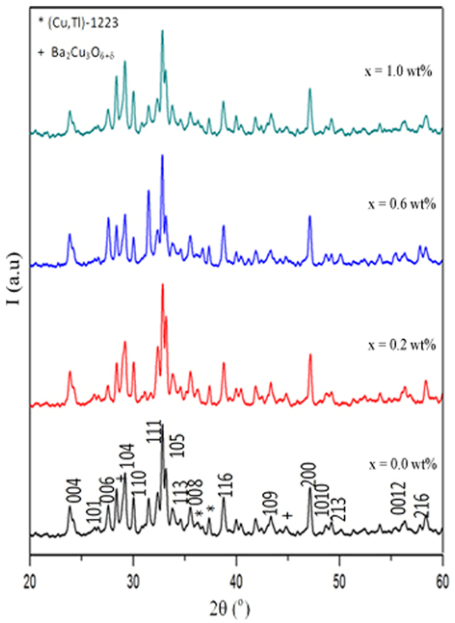

Fig. 1 XRD patterns for $(MgO)_x Cu_{0.25}Tl_{0.75}Ba_2Ca_3Cu_4O_{12-\delta}$ superconducting samples ($x = 0.0$, 0.2, 0.6 and 1.0 wt%)

3 Results and Discussion

The room-temperature X-ray powder diffraction patterns for $(MgO)_x Cu_{0.25}Tl_{0.75}Ba_2Ca_3Cu_4O_{12-\delta}$ superconducting samples ($x = 0.0$, 0.2, 0.6 and 1.0 wt%) are shown in Fig. 1. The major lines of the diffraction patterns are well indexed by a tetragonal unit cell of (Cu, Tl)-1234 with space group P4/mmm. The volume fraction of the samples prepared, estimated from the peak intensities of the same particular reflections [23], increases from 88% to 96% as x increases from 0.0 to 0.6 wt% and then decreases to 82% as x reaches 1.0 wt%. Some impurities like that observed by Badica et al. [24], $Ba_2Cu_3O_{5+\delta}$ and (Cu, Tl)-1223, are found in small amounts. Also, no patterns corresponding to MgO and/or Mg-rich compounds were detected in XRD up to 1.0 wt%. The EDS analysis for $x = 1.0$ wt% sample showed the existence of Mg in the bulk sample between the superconducting grains as shown in Fig. 2. A similar result was observed in $(Bi,Pb)_2Sr_2Ca_2Cu_3O_{10-\delta}$ superconducting phase added by nano MgO [25]. So the effect of MgO on (Cu, Tl)-1234 phase can be considered as a catalyst role changing the rate of reaction that retards the (Cu, Tl)-1234 phase formation. The change in the rate of reaction could be related to the change in the viscosity of the forming transient liquid at the reaction temperature, which in turn affects its homogeneity and hence the formation rate of (Cu, Tl)-1234 phase [7].

SEM images for $(MgO)_x Cu_{0.25}Tl_{0.75}Ba_2Ca_3Cu_4O_{12-\delta}$ superconducting samples with $x = 0.0$, 0.2, 0.6, and 1 wt% are shown in Figs. 3a to 3d, respectively. More grains with regular plate-like or bar-like are observed in $x = 0.0$, 0.2 and 0.6 wt% samples, indicating the formation of (Cu, Tl)-1234

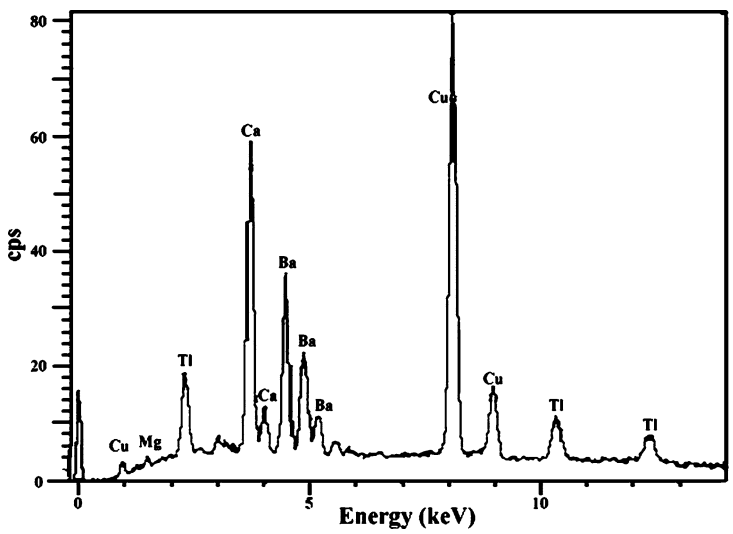

Fig. 2 Typical EDS analysis for $(MgO)_x Cu_{0.25}Tl_{0.75}Ba_2Ca_3Cu_4O_{12-\delta}$ with $x = 1.0$ wt%

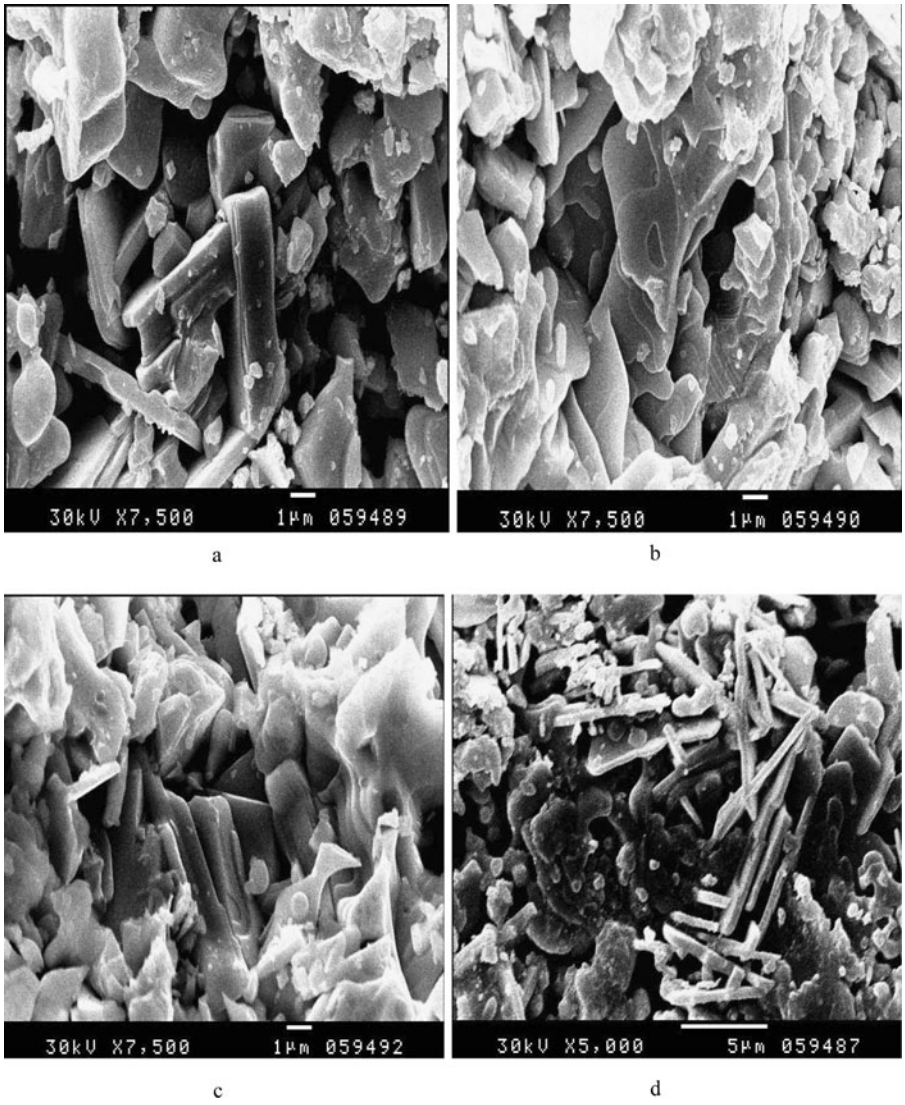

Fig. 3 SEM images for $(MgO)_x Cu_{0.25}Tl_{0.75}Ba_2Ca_3Cu_4O_{12-\delta}$ superconducting samples: (**a**) $x = 0.0$ wt%, (**b**) $x = 0.2$ wt%, (**c**) $x = 0.6$ wt%, (**d**) $x = 1.0$ wt%

phase [24]. Some blocks of several composed plates or bars are also observed, especially in $x = 0.6$ wt% sample. This means that MgO nano-oxides addition up to $x = 0.6$ wt% can heal microcracks and increase the connectivity between the grains in $(Cu_{0.25}Tl_{0.75})$-1234 phase. The grain size decreases as x increases, indicating that the spherical MgO grains act as a barrier and hinders the grains growth. Furthermore, in $x = 1.0$ wt% sample, the spherical MgO grains are observed clearly between the superconducting grains, indicating that MgO particles remain as discrete nano-particles even after sintering process.

The variation of the electrical resistivity with temperature for $(MgO)_x Cu_{0.25}Tl_{0.75}Ba_2Ca_3Cu_4O_{12-\delta}$, with $x = 0$, 0.2, 0.4, 0.6, 0.8 and 1.0 wt%, is shown in Fig. 4. All the samples show metallic-like behavior from room temperature down to onset of superconductivity. A higher value of the normal-state resistivity are recorded for $x = 0.4$ wt% sample, whereas a lower value is recorded for samples of $x = 0.6$ wt% sample which is closer to that of the pure sample. The normal-state resistivity may strongly depend on porosity and grain boundaries scattering. These results are consistent with SEM results which show that $x = 0.6$ wt% sample has the lowest porosity. On the other hand, The superconducting transition temperature calculated from resistivity data increases from 122 to 136 K as x increases from 0.0 to 0.8 wt% and then it decreases to 117 K with $x = 1.0$ wt% as shown in the inset of Fig. 4.

To provide more evidence concerning these measurements, the dielectric properties, such as real ε' and imaginary ε'' parts of dielectric constant, dielectric loss $\tan\delta$, and ac conductivity σ_{ac} for $(MgO)_x Cu_{0.25}$,$Tl_{0.75}Ba_2Ca_3Cu_4O_{12-\delta}$ with $x = 0.0$, 0.2, 0.4, 0.6, 0.8 and 1.0 wt% are measured in the frequency range from 100 Hz to 4 MHz at different temperatures from 113 to 300 K. The variation of ε' with frequency at different temperatures for $x = 0.0$ wt% sample is shown in Fig. 5. In general the curve shows the

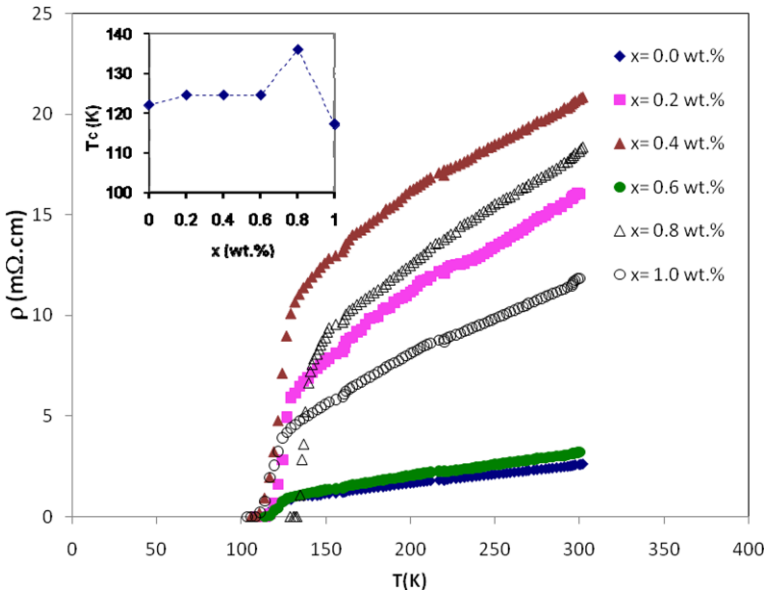

Fig. 4 The variation of the electrical resistivity with temperature for $(MgO)_x Cu_{0.25}Tl_{0.75}Ba_2Ca_3Cu_4O_{12-\delta}$, with $x = 0$, 0.2, 0.4, 0.6, 0.8 and 1 wt%. The inset shows the variation of T_c with x

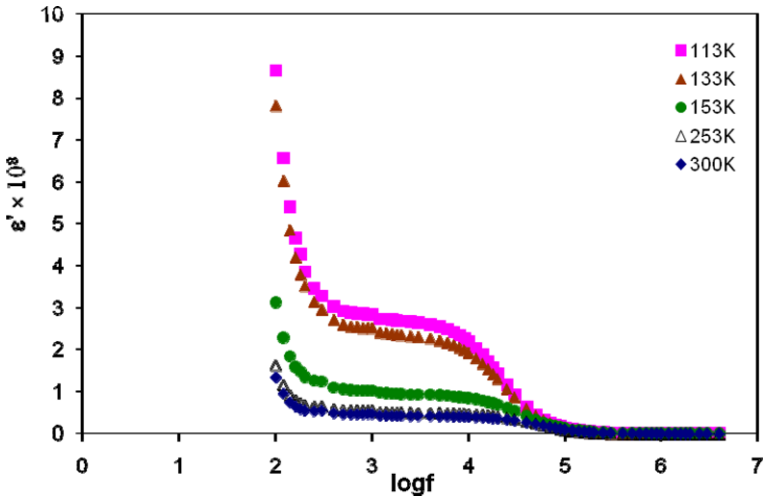

Fig. 5 The variation of the dielectric constant of $Cu_{0.25}Tl_{0.75}Ba_2Ca_3Cu_4O_{12-\delta}$ sample with frequency at different temperatures

contribution of individual polarization mechanisms to the dielectric constant and their relaxation frequencies. As each process relaxes, ε' becomes smaller because the contribution to polarization from that mechanism ceases.

At low frequencies, all four sources of polarization (electronic, ionic, dipolar and space charge polarization) are dominant. The strong increase of ε' as detected at lower frequencies (10^3 Hz) corresponds to Maxwell–Wagner-like effects and attributed to the interfacial polarization due to inhomogeneous dielectric structure [26–28]. These take place at the grain boundaries and/or at the electrode contacts. Space charge polarization at the electrodes is also considered as a one of factors that increases ε' at low frequencies. As the frequency increases (10^3–10^4 Hz), the available time for the drift of charge carriers is reduced and the observed increase in ε' is substantially less. In this case the polarizability is associated with the material rather than the interface and ε' decreases [29]. With further increase in f (10^4–10^5 Hz), ε' decreases rapidly. This can be explained according to the oscillation of the applied field is too fast and the dipolar polarization characteristic time is longer than the time constant of the applied field [21]. So the decrease of ε' is due to the reduction in dipolar polarization role. Beyond 1 MHz, the dielectric constant ε' becomes temperature independent. This indicates that at high frequencies, the dielectric constant response results from the sample in the absence of dipolar polarization. Therefore, it could be suggested that the dielectric constant mainly originates from electronic and lattice polarization contributions on account of their short relaxation time [8]. Regarding the effect of the temperature, ε' decreases as temperature increases, which could be related to the decrease in polarizability.

The variation of ε' with frequency at room temperature for different x is shown in Fig. 6. In the low radio frequency (kHz), ε' increases to the largest value for $x = 0.4$ wt% which could be related to the existence of secondary phases,

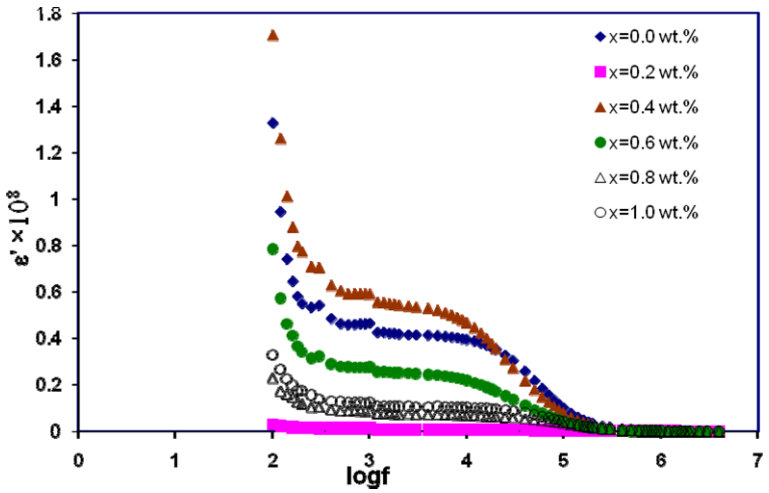

Fig. 6 The variation of the dielectric constant, ε' with frequency at room temperature for $(MgO)_x Cu_{0.25}Tl_{0.75}Ba_2Ca_3Cu_4O_{12-\delta}$ samples with $x = 0.0$, 0.2, 0.4, 0.6, 0.8 and 1 wt%

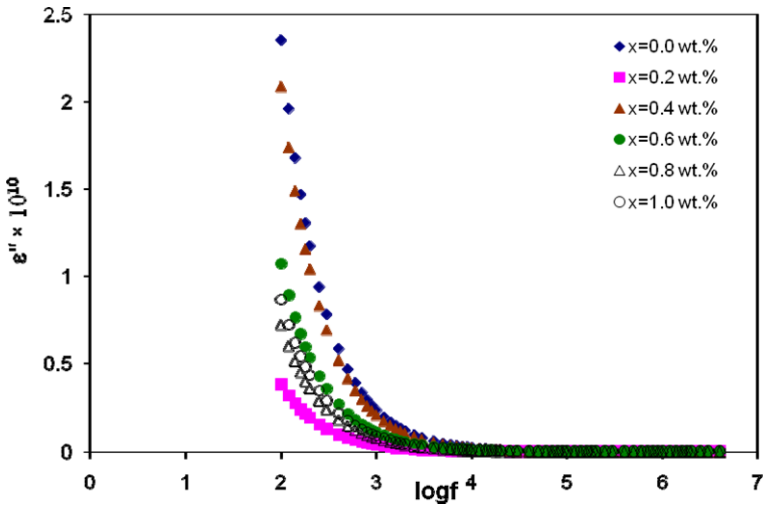

Fig. 7 The variation of the imaginary part, ε'' with frequency for $Cu_{0.25}Tl_{0.75}Ba_2Ca_3Cu_4O_{12-\delta}$ sample at different temperatures

impurities and grain boundaries scattering. This confirmed the largest resistivity value of this sample. For further increase in x, ε' is decreased which could be attributed to the effect of MgO in the increasing of volume fraction of the main phase, the healing of microcracks and increase the connectivity between the grains, the improving in the microstructures of the samples and relatively reduction in both impurities and electrical inhomogeneity.

The variation of the imaginary part of dielectric ε'' with frequency, for $(MgO)_x Cu_{0.25}Tl_{0.75}Ba_2Ca_3Cu_4O_{12-\delta}$ samples with different x values at room temperature, is shown in Fig. 7. It is clear that all the studied samples exhibit the dielectric dispersion where ε'' decreases as the frequency increases from 100 Hz–4 MHz. It decreases rapidly in the low-frequency region and the rate of decrease is slow in high frequency region, the behavior almost approaches to frequency independent behavior. The phenomenon of dielectric dispersion has been explained on the basis of Maxwell–Wagner model [30] and Koop's phenomenological theory [31] of dielectrics. In this model, a dielectric medium has been assumed to be made of well conducting grains, which are separated by poorly conducting grain boundaries. Therefore the grains are highly conductive and have high values of permittivity, while the grain boundaries are less conductive and have smaller values of permittivity. At lower frequencies the grain boundaries are more effective than electrical conduction grains. The variation of the loss factor with frequency for $Cu_{0.25}Tl_{0.75}Ba_2Ca_3Cu_4O_{12-\delta}$ sample at different temperatures is shown in Fig. 8. The dispersion in $\tan\delta$ is found to shift toward higher frequencies as the temperature increases. This behavior is clearer in the inset where $\tan\delta$ was calculated using the series capacitance and was plotted against $\log f$. In this case peaks appeared corresponding to dispersion positions indicating the relaxation process. At the peak, the relaxation time of the electrical dipoles is close to the period of the applied electric field, resulting in the maximum of dissipation. The shift of the peak toward higher frequencies as the temperature increases could be attributed to the relaxation time decreases with increasing temperature. Such dielectric response indicates a Debye-like

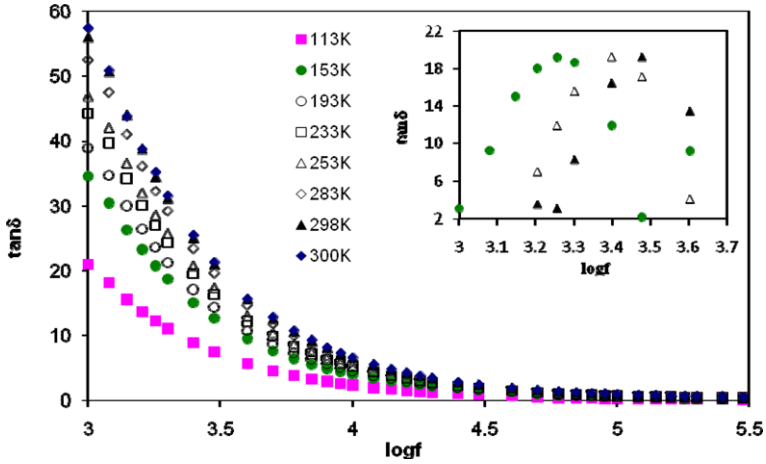

Fig. 8 The variation of the loss factor with frequency for $Cu_{0.25}Tl_{0.75}Ba_2Ca_3Cu_4O_{12-\delta}$ sample at different temperatures. The inset shows $\tan\delta$ as calculated using the series capacitance vs. $\log f$

Table 1 The variation of τ with T and x

T (K)	$10^{-4} \times \tau$ (s)					
	$x = 0.0$ wt%	$x = 0.2$ wt%	$x = 0.4$ wt%	$x = 0.6$ wt%	$x = 0.8$ wt%	$x = 1$ wt%
113	1.592	0.227	2.2748	1.327	0.5308	0.6369
153	0.8846	0.0995	1.327	1.1374	0.5308	0.5308
213	0.7962	0.0796	0.9952	0.8846	0.3981	0.3981
253	0.6369	0.0637	0.8846	0.7962	0.3185	0.3981
298	0.5308	0.0531	0.7962	0.6369	0.2654	0.3185

relaxation process. The broad $\tan\delta$ peak suggests that there exists different dipolar relaxation time τ. This implies additional spatial charge polarizations due to the electrical inhomogeneity in the interfaces, grain boundaries, or caves. It is expected that the effect can be suppressed by improving the microstructures of the samples [8].

At the relaxation frequency, the most probable relaxation time, τ is obtained and given by

$$\omega\tau = 1 \tag{5}$$

where ω is the angular frequency corresponding to the peak in $\tan\delta$. According to the Debye model, the dipolar polarization relaxation time obeys the Arrhenius relation,

$$\tau = \tau_\sigma e^{(U/K_B T)} \tag{6}$$

where U represents the activation energy required for the relaxation and τ_0 is a pre-exponential factor. The most probable relaxation time, τ, obtained according to (5) for $(MgO)_x Cu_{0.25}Tl_{0.75}Ba_2Ca_3Cu_4O_{12-\delta}$ are displayed in Table 1 with different T and x. It decreases as temperature increases. The $\ln\tau$ versus $1/T$ which show activated behavior, (6), is shown in Fig. 9 for $x = 0.2$ wt% sample. A linear regression of the data yields the values $U \sim 22$ meV and $\tau_0 \sim 23 \times 10^{-7}$ s. U values for all other samples are shown in Fig. 10. U is of order around 20 meV which comparable with that for CCTO [9] and much smaller than that of Bi-2222 [8].

The variation of ac conductivity with frequency at different fixed temperatures for $Cu_{0.25}Tl_{0.75}Ba_2Ca_3Cu_4O_{12-\delta}$ is shown in Fig. 11. In low-frequency regime, ac conductivity decreases with increase in temperature indicating dispersion of conductivity with temperature. With increase in frequency, the dispersion in conductivity narrowed and all the curves for different temperature appeared to merge into a single curve at high frequencies. $\sigma_{ac}(\omega)$ exhibits power law behavior and the data yield $\sigma_{ac}(\omega) \sim \omega^{-\gamma}$ with $\gamma \approx 0.8$. AC conductivity may arise due to free as well as bound carriers. When the ac conductivity increases with increasing frequency, the conductivity must be related to the bound carriers trapped in the sample. If the conduction is due to free carriers then the conductivity must decrease with increase in frequency [32]. As the ac conductivity data in Fig. 11 decrease with increasing frequency, the observed ac conductivity must be related to the free carriers. The same behavior was obtained for the cuprate superconductors $Bi_2Sr_2Ca_2Cu_3O_{10}$, $Bi_2Sr_2CaCu_2O_8$ and $YBa_2Cu_3O_{6.95}$ with $\gamma \approx 0.7$ in infrared frequency range [33, 34].

4 Conclusion

MgO nano-oxide addition increased the volume fraction of the prepared samples. It can heal microcracks and increased the connectivity between the grains. T_c increased from 122

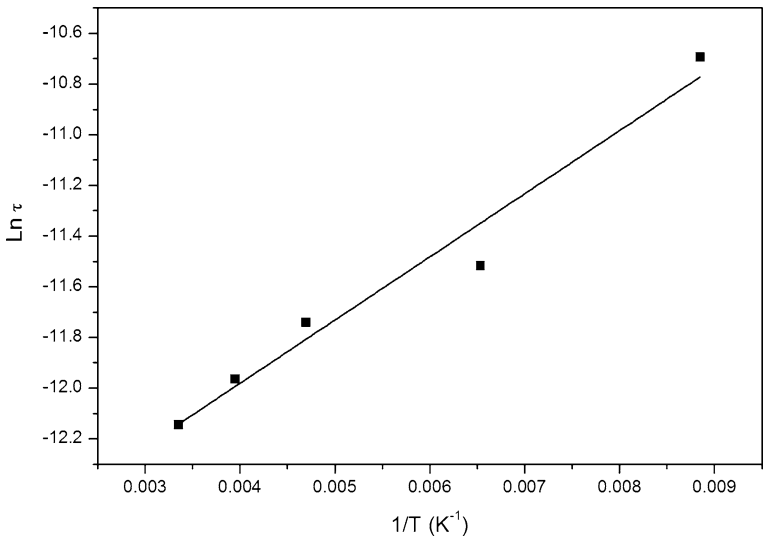

Fig. 9 The variation of $\ln \tau$ with $1/T$ for $(MgO)_x Cu_{0.25}Tl_{0.75}Ba_2Ca_3Cu_4O_{12-\delta}$ sample with $x = 1$ wt%

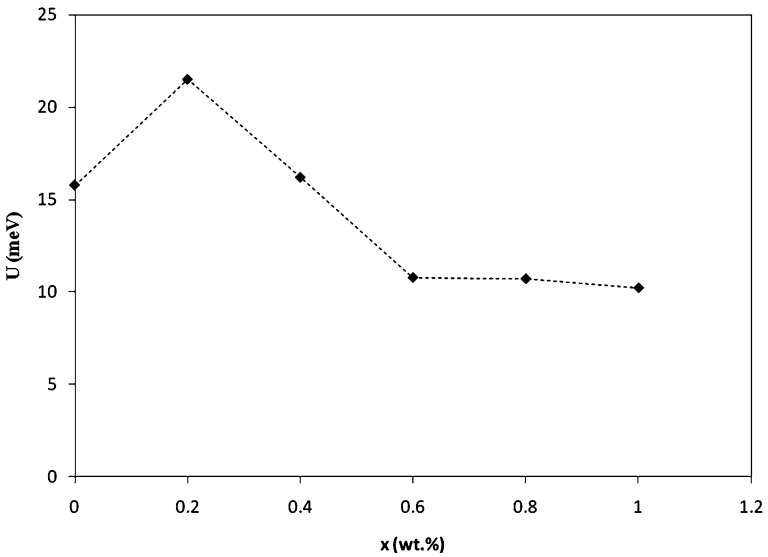

Fig. 10 The variation of the activation energy U with x

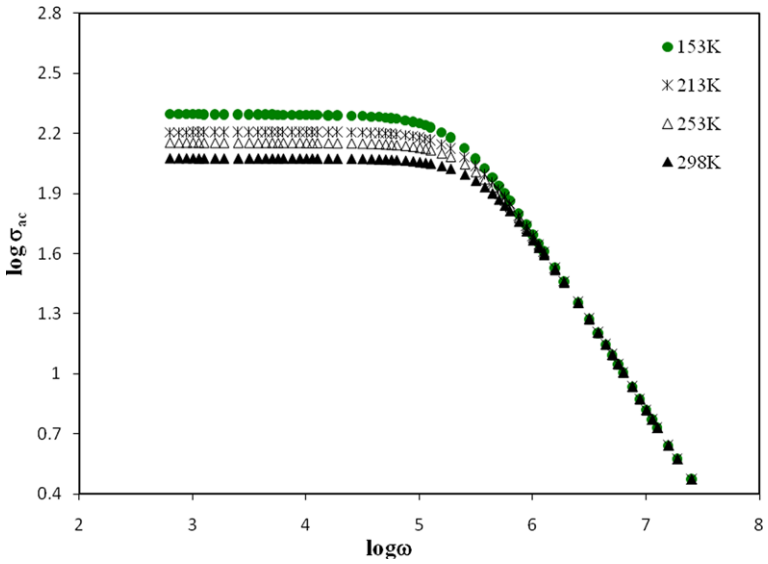

Fig. 11 The variation of ac conductivity of $Cu_{0.25}Tl_{0.75}Ba_2Ca_3Cu_4O_{12-\delta}$ sample with angular frequency at different temperatures

to 136 K as x increased from 0.0 to 0.8 wt%. In the low radio frequency (kHz), ε' increased to the largest value for $x = 0.4$ wt%, which could be related to the existence of secondary phases, impurities and grain boundaries scattering consistent with the largest resistivity recorded. For further increase in x, ε' was decreased which could be attributed to the effect of MgO in the increasing of volume fraction of the main phase, the healing of microcracks and increase the connectivity between the grains, the improving in the microstructures of the samples and relatively reduction in both impurities and electrical inhomogeneity. The imaginary part of dielectric constant ε'' and loss factor $\tan\delta$ showed dispersion which shift toward lower frequencies with decreasing temperature. Such dielectric response indicated a Debye-like relaxation process. AC conductivity, σ_{ac} was derived from the admittance and sample dimensions in the same frequency range. It followed the power low $\sigma_{ac}(\omega) \sim \omega^{-\gamma}$ with $\gamma \approx 0.8$. As the ac conductivity decreases with increasing frequency, therefore, the observed ac conductivity was related to the free carriers. The conduction mechanism was suggested to be due to translation of free carriers.

Acknowledgements This work was performed in Physics Department, Faculty of Science, Alexandria University, Alexandria, EGYPT. Thanks are due to Prof. Dr. A.I. Abou-Aly, Chairman of Superconductivity and Metallic Glasses Group at Physics Department, Faculty of Science, Alexandria University, Alexandria, EGYPT. Also thanks are due to Prof. Dr. R. Awad for his support and help. The author thanks Miss A. Abd El-Wanis for her help during preparation of the samples.

References

1. Khan, N.A., Khurram, A.A., Javed, A.: Physica C **422**, 9 (2005)
2. Ihara, H., Tokiwa, K., Tanaka, K., Tsukamoto, T., Watanabe, T., Yamamoto, H., Iyo, A., Tokumoto, M., Umeda, M.: Physica C **282–287**, 957 (1997)
3. Ihara, H., Tanaka, K., Tanaka, Y., Iyo, A., Terada, N., Tokumoto, M., Ariyama Hase, M., Sundaresan, A., Hamada, N., Miyashita, S., Tokiwa, K., Watanabe, T.: Physica C **341–348**, 487 (2000)
4. Khan, N.A., Sekita, Y., Terada, N., Ihara, H.: Supercond. Sci. Technol. **14**, 603 (2001)
5. Khan, N.A., Husnain, G.: Physica C **436**, 51 (2006)
6. Mohammed, N.H., Roumié, M., Motaweh, H.A., Awad, El-Said Bakeer, D., Nsouli, B.: J. Supercond. Nov. Magn. **23**(1), 465 (2010)
7. Awad, R.: J. Supercond. Nov. Magn. **21**, 461 (2008)
8. Xu, X., Jiao, Z., Fu, M., Feng, L., Xu, K., Zuo, R., Chen, X.: Physica C **417**, 166 (2005)
9. Homes, C.C., Vogt, T., Shapiro, S.M., Wakimoto, S., Ramirez, A.P.: Science **293**, 673 (2001)
10. Cavdar, S., Koralay, H., Tugluoglu, N., Gunen, A.: Supercond. Sci. Technol. **18**, 1204 (2005)
11. Nkum, R.K., Gyekye, M.O., Boakye, F.: Solid State Commun. **122**, 569 (2002)
12. Konopka, J., Jose, R., Wolcyrz, M.: Physica C **435**, 53 (2006)
13. Mazzara, G.P., Skirius, S., Cao, G., Chern, G., Clark, R.J., Crow, J.E., Mathias, H., O'Reilly, J.W., Testardi, L.R.: Phys. Rev. B **47**, 8119 (1993)
14. Rey, C.M., Mathias, H., Testardi, L.R., Skirius, S.: Phys. Rev. B **45**, 10639 (1992)
15. Reagor, D., Ahrens, E., Cheong, S.-W., Migliori, A., Fisk, Z.: Phys. Rev. Lett. **62**, 2048 (1989)
16. Cao, G., O' Reilly, J.W., Crow, J.E., Testardi, L.R.: Phys. Rev. B **47**, 11510 (1993)
17. Testardi, L.R., Moulton, W.G., Mathias, H., Ng, H.K., Rey, C.M.: Phys. Rev. B **37**, 2324 (1988)
18. Chen, J.W., Wang, J.C., Chen, Y.F.: Physica C **289**, 131 (1997)
19. Shi, J.B.: Physica C **305**, 35 (1998)
20. Awad, R.: J. Alloys Compd. **474**, 517 (2009)
21. Mumtaz, M., Khan, N.A.: Physica C **469**, 182 (2009)
22. Mumtaz, M., Khan, N.A.: Physica C **469**, 728 (2009)
23. Karaca, I., Celebi, S., Varilci, A., Malik, A.I.: Supercond. Sci. Technol. **16**, 100 (2003)
24. Badica, P., Iyo, A., Crisan, A., Ihara, H.: Supercond. Sci. Technol. **15**, 975 (2002)
25. Guilmeau, E., Andrzejewski, B., Noudem, J.G.: Physica C **387**, 382 (2003)
26. Lunkenheimer, P., Bobnar, V., Pronin, A.V., Ritus, A.I., Volkov, A.A., Loidl, A.: Phys. Rev. B **66**, 052105 (2002)
27. Lunkenheimer, P., Fichtl, R., Ebbinghaus, S.G., Loidl, A.: Phys. Rev. B **70**, 172102 (2004)
28. Krohns, S., Lunkenheimer, P., Ebbinghaus, S.G., Loidl, A.: Appl. Phys. Lett. **91**, 022910 (2007)
29. Kaur, D., Narang, S.B., Thind, K.S.: J. Ceram Process. Res. **7**(1), 31 (2006)
30. Wagner, K.W.: Ann. Phys. **40**, 817 (1913)
31. Koops, C.G.: Phys. Rev. **83**, 121 (1951)
32. Kamalasanan, M.N., Deepak Kumar, N., Chandra, S.: J. Appl. Phys. **74**, 5679 (1993)
33. El Azrak, A., Nahoum, R., Bontemps, N., GuillouxViry, M., Thivet, C., Perrin, A., Labdi, S., Li, Z.Z., Raffy, H.: Phys. Rev. B **49**, 9846 (1994)
34. Puchkov, A.V., Basov, D.N., Timusk, T.: J. Phys., Condens. Matter **8**, 10049 (1996)